
Article:
Zhang, X, Hou, Y, Ettelaie, R orcid.org/0000-0002-6970-4650 et al. (4 more authors) (2019) Pickering Emulsion-Derived Liquid–Solid Hybrid Catalyst for Bridging Homogeneous and Heterogeneous Catalysis. Journal of the American Chemical Society, 141 (13). pp. 5220-5230. ISSN 0002-7863

https://doi.org/10.1021/jacs.8b11860

Supporting Information

A Pickering Emulsion-Derived Liquid-Solid Hybrid Catalyst for Bridging Homogeneous and Heterogeneous Catalysis

Xiaoming Zhang,[†,§] Yiting Hou,[†,§] Rammile Ettelaie,[#] Ruqun Guan,[†] Ming Zhang,[†] Yabin Zhang[†] and Hengquan Yang*[†]

[†] *School of Chemistry and Chemical Engineering, Shanxi University, Taiyuan 030006, China*

[#] *Food Colloids Group, School of Food Science and Nutrition, University of Leeds, Leeds LS2 9JT, U.K.*

*To whom correspondence should be addressed: hqyang@sxu.edu.cn

Experimental Section

Figure S1. Characterizations of silica emulsifier

Figure S2. Appearance of a water droplet in air on a disk of compressed silica nanoparticles

Figure S3. Optical micrographs for Pickering emulsions and their droplet size distributions

Figure S4. SEM images of liquid-solid hybrid capsules with different particle sizes fabricated by tuning the shearing speed

Figure S5. SEM images of the liquid-solid hybrid capsules with different crust thicknesses by tuning the TMS amount

Figure S6. N_2 sorption characterization of the hybrid capsules with different crust thicknesses by tuning the TMS amount

Figure S7. Fluorescence microscopy with time for the transport of FITC-I out of liquid-solid hybrid capsules

Figure S8. Flow behavior and mechanical stability for the IL-in-oil Pickering emulsions in a column reactor

Figure S9. Comparison of thermal stability between liquid-solid hybrid capsules and Pickering emulsions

Figure S10. Behavior and tolerance of the Pickering emulsion in methanol

Figure S11. Confocal fluorescence microscopy for the distribution of Rhodamine B-labeled enzyme within liquid-solid hybrid capsules

Figure S12. Kinetic profiles and specific activity for the CALB-catalyzed kinetic resolution of alcohols over the liquid-solid hybrid catalyst in continuous-flow system and over CALB in batch reaction system

Figure S13. Lilly-Hornby plot and Lineweaver-Burk plot

Figure S14. The kinetic plots of Cr^{III}(salen)-catalyzed ARO of cyclopentene oxide in batch reaction system

Figure S15. Pd-catalyzed allylic substitution reactions in batch system and in the liquid-solid hybrid catalyst based flow system

Mass Spectrometry Spectra and Nuclear Magnetic Spectra

Experimental Section

1. Chemicals

All chemicals were used as received unless otherwise stated. Fumed silica nanoparticles N20 (20 nm) was purchased from Wacker Chemie. Dimethyldichlorosilane, (*R, S*)-1-phenylethyl alcohol (98%), vinyl acetate (99%), rhodamine B (99%), trimethoxysilane (TMS), tetramethoxysilane (TMOS), $Pd(OAc)_2$ and fluorescein isothiocyanate isomer I (FITC-I, CAS No.3326-32-7) were purchased from Aladdin (China). (*R, S*)-4-phenyl-2-butanol (98%) was purchased from Adamas Reagent Co., Ltd, (China). (*R, S*)-1-Indanol (98%), trimethylsilyl azide ($TMSN_3$), Nile Red (CAS No. 7385-67-3) and (*R, S*)-4-methyl-2-pentanol (99%) were purchased from Alfa Aesar. 1,2-epoxybutane, 1,2-epoxyhexane, 1,2-epoxyoctane, 2,3-epoxybutane, cyclopentene oxide, cyclohexene oxide and triphenyl phosphine-3,3',3''-trisulfonic acid trisodium salt (TPPTS) were purchased from Beijing Innol-Chem. Native Lipase B from *Candida Antarctica* (CALB) was purchased from Novozymes. 1-Butyl-3-methylimidazolium hexafluorophosphate (99%) and 1-butyl-3-methylimidazolium tetrafluoroborate (99%) were purchased from Lanzhou Institute of Chemical Physics, Chinese Academy of Sciences. *n*-Octane, morpholine and piperidine were purchased from Shanghai Chemical Reagent Company of the Chinese Medicine Group. Water used in this study was de-ionized water. Cr^{III}(salen) was synthesized according to the previous literature report [*J. Am. Chem. Soc.*, 1998, 120 (41), 10780-10781]. (*E*)-1,3-diphenylallyl acetate was synthesized according to a literature report [Dalton Transactions, 2017, 46, 1510-1519].

2. Characterization

Emulsion droplets were observed using an optical microscope analyzer (XSP-8CA, Shanghai, China) equipped with 4 or 10 × magnification lens. Confocal laser scanning microscopy images were obtained on a Carl Zeiss LSM880 instrument (Germany). The contact angles of water in air on silica particle disks were measured using a Krüss DSA100 instrument. Before measurement, the powder sample was compressed into a disk of thickness approximately 1 mm (*ca.* 2 MPa). The appearance of the water droplet on the disk was recorded at *ca*. 0.1 s with a digital camera. The value of the contact angle was determined by a photogoniometric method. Thermogravimetric (TG) analysis was performed under an air atmosphere with a heating rate of 10 °C/min by using a SDT Q600 thermogravimetric analyzer. Nitrogen-sorption analysis was performed at -196 °C on a Micromeritics ASAP 2020 analyzer. Before measurement, samples were out gassed at 120 °C under vacuum for 4 h (for liquid-solid hybrid samples, the ILs were washed out by methanol before vacuum treatment). The specific surface area was calculated from the adsorption branch in the relative pressure range of 0.05–0.15 using Brunauer-Emmett-Teller (BET) method. The total pore volume was estimated from the amount adsorbed at the P/P_o value of 0.99. Pore size distributions were determined from the adsorption branches using a BJH method. Scanning electron microscope (SEM) images were performed using a Hitachi SU 1510. For the observation of crust thickness, IL was removed by methanol firstly. Transmission electron microscopy (TEM) was performed on a JEOL-JEM-2000EX microscope. Samples for TEM observation were prepared by dispersing the sample powder in ethanol using ultrasound and then allowing a drop of the suspension to evaporate on a copper gird covered with a holey carbon film. Gas chromatography (GC) analysis was carried out on an Agilent 7890 analyzer (Agilent-19091G-B213, HP-CHIRAL-20B) with a flame ionization detector. High performance liquid chromatography (HPLC) analysis was performed on Shimadzu LC-20AT equipped with a UV-detector using *n*-hexane and isopropanol as moving phase (V/V=95/5, rate 1.0 mL/min). GC-MS analysis was performed on an Agilent 7890-5977A MSD with HP-5 as column. Nuclear magnetic resonance (NMR) spectra were recorded on a Bruker AC 400 spectrometer using $CDCl_3$ as the solvent.

3. Material Synthesis

Preparation of silica emulsifier. Commercial silica nanoparticles (1.0 g, 20 nm in diameter, dried at 120 °C for 4 h) were dispersed into 30 mL toluene. Then, 3 mmol $(CH_3)_2SiCl_2$ and 6 mmol $CH_3(CH_2)_5NH_2$ (as catalyst) were added into this suspension. The mixture was stirred under a N_2 atmosphere at 60 °C for 4 h. The solid particles were collected

through centrifugation, and throughly washed with toluene and methanol. Dimethyl-modified silica particles were obtained as emulsifiers after drying.

Preparation of IL-in-oil Pickering emulsions. 1 mL of oil phase (octane) containing silica emulsifier (20 mg) was added into a mixture of ionic liquids (0.75 g [BMIM]PF_6, 0.20g [BMIM]BF_4 and 0.05 g water). After vigorous shearing the mixture at a given speed (5000, 15000 or 20000 rpm for 1.5 min) by a homogenizer, IL-in-oil Pickering emulsions were generated.

Preparation of FITC-I-labelled IL-in-oil Pickering emulsions. The procedures were similar with the formation of IL-in-oil Pickering emulsions except that 0.01 mmol FITC-I was dissolved into the IL mixture.

General procedure for preparing liquid-solid hybrid capsules. The above resulted IL-in-oil Pickering emulsion was dispersed into 19 mL *n*-octane that containing a given amount of trimethoxysilane (TMS, 0.04, 0.08 or 0.12 g). The mixture was rotated on a rolling apparatus at 50 °C for 12 h. Then, the above octane phase was removed and the solid capsules were washed with octane for several times. The resulted hybrid material was re-dispersed in octane for the following packing in a column reactor. Liquid-solid hybrid capsules hosting CALB were prepared with similar procedures except that a given amount of CALB was introduced by dissolving them in IL before emulsification. For Cr^{III}(salen)- or $Pd(OAc)_2$-loaded liquid-solid hybrid capsules, the synthesis procedures were also similar with above except that TMOS was utilized as a cross-linking reagent.

Preparation of liquid-solid hybrid capsules with different particle sizes. The shearing speed for emulsification was tuned from 5000 to 15000, 20000 rpm. The amount of cross-linking reagent TMS was fixed at 0.08 g.

Preparation of liquid-solid hybrid capsules with different permeability (crust thickness). The liquid-solid hybrid microcapsules with different membrane thickness were obtained by tuning the amount of cross-linking reagent TMS (0.04, 0.08 or 0.12 g), and the shearing speed was kept at 15000 rpm.

Preparation of FITC-I-labelled liquid-solid capsules. FITC-I-labelled IL-in-oil Pickering emulsions were used, and the amount of cross-linking reagent TMS was varied from 0.04 to 0.08, 0.12 g.

4. **Permeability of Liquid-Solid Hybrid Capsules.** The liquid-solid hybrid capsules were deposited on a glass slide and diluted with *n*-octane. 5 μL Nile Red solution (2.5 μM in *n*-octane) was gently dropped on the glass slide. The diffusion of Nile Red molecules into liquid-solid hybrid capsules was recorded by fluorescence microscopy at intervals. Similarly, FITC-I-containing capsules were deposited on a glass slide and 100 μL a mixture of ethanol and water (20 % v/v) was gently dropped onto the glass slide. The diffusion of FITC-I out of the capsules was recorded by fluorescence microscopy at intervals.

5. **The Mechanical Stability Tests.** The liquid-solid hybrid capsules prepared at 15000 rpm with 0.08 g TMS were utilized, and packed into a column. *n*-Octane was chosen as a flow phase. The inner pressure of the column was tuned to 1 MPa by pump. For comparison, the stability of an IL-in-oil Pickering emulsion was also tested by filling the emulsion into a column and performing the similar operation.

6. Catalytic Reactions in Continuous-Flow Reaction System or Batch Biphasic Reaction System

CALB-catalyzed kinetic resolution of alcohols in continuous-flow reaction systems. Typically, a suspension of the CALB-containing liquid-solid hybrid catalyst (for example 5.0 g) in *n*-octane was poured into a column reactor (inner diameter is 2 cm), whose bottom is a sand filter (4.5–9 μm in pore diameter). A solution of racemic alcohol (for example 0.35 M) and vinyl acetate (for example 1.4 M) in *n*-octane as mobile phase was pumped through the inlet of the column reactor at a given flow rate and was allowed to pass through the column reactor whose temperature was kept at 45 °C. The outflow was sampled for GC analysis at intervals.

Cr^{III}(salen)-catalyzed ARO reactions of epoxides in continuous-flow reaction systems. A suspension of the Cr^{III}(salen)-containing liquid-solid hybrid catalyst in *n*-octane was gently poured into a column reactor. A solution of

epoxide (0.04 M) and $TMSN_3$ (0.0.044 or 0.024 M) in *n*-octane as mobile phase was pumped through the inlet of the column reactor at a given flow rate and was allowed to pass through the column reactor. The outflow was collected for GC analysis at intervals.

Pd-catalyzed allylic substitution in continuous-flow reaction systems. A suspension of the $Pd(OAc)_2$-containing liquid-solid hybrid catalyst in *n*-octane was gently poured into a column reactor. A solution of (*E*)-1,3-diphenylallyl acetate (0.12 M) and morpholine or piperidine as N-nucleophiles (0.18 M) in *n*-octane as mobile phase was pumped through the inlet of the column reactor. The outflow was collected for HPLC analysis at intervals.

CALB-catalyzed kinetic resolution of alcohols in batch biphasic reaction systems. Typically, a mixture of 1.5 g [BMIM]PF_6 and 0.4 g [BMIM]BF_4, 40 μL aqueous enzyme solution (4 mg mL^{-1} of protein; pH 8.0), 1.0 mL *n*-octane solution of racemic alcohols (for example 0.1 M) and vinyl acetate (0.4 M) were charged into a vial. The reaction mixture was stirred with a magnetic bar (10 mm in length, 3000 rpm) at 45 °C. Aliquots of the solution were taken at intervals and extracted with diethyl ether for monitoring conversions by chiral GC analysis.

Cr^{III}(salen)-catalyzed ARO reactions of epoxides in batch biphasic reaction systems. A mixture of 0.8 g [BMIM]PF_6 and 0.2 g [BMIM]BF_4, 30 mg Cr^{III}(salen), 2.5 mL *n*-octane solution of cyclopentene oxide (0.10 M) and $TMSN_3$ (0.11 M) were charged into a vial. The reaction mixture was stirred with a magnetic bar at room temperature. Aliquots of the solution were taken at intervals for monitoring conversions and ee values by chiral GC analysis.

Pd-catalyzed allylic substitution in batch biphasic reaction systems. A mixture of 1.0 g [BMIM]BF_4, 0.03 mmol $Pd(OAc)_2$, 0.12 mmol TPPTS, 1.5 mL *n*-octane solution of (*E*)-1,3-diphenylallyl acetate (0.12 M) and morpholine (0.18 M) were charged into a vial. The reaction mixture was stirred with a magnetic bar at room temperature. Aliquots of the solution were taken at intervals for monitoring conversions by HPLC analysis.

7. Detailed Definitions and Derivation Processes of Equations for Theoretical Investigation of the Impact of Enzyme Loading.

Definitions

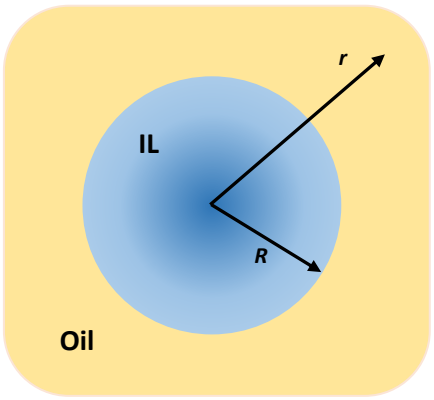

R – Radius of IL pool

r – Distance from centre of IL pool

K_1 – Rate constant of forward reaction in IL

K_2 – Rate constant of backward reaction in IL

A – Concentration of reactant A

B – Concentration of reactant B

C – Concentration of product C

A_O^0 – Initial concentration of A in oil phase

B_O^0 – Initial concentration of B in oil phase

C_O^0 – Initial concentration of C in oil phase

A_{IL}^0 – Initial concentration of A in IL phase

B_{IL}^0 – Initial concentration of B in IL phase

C_{IL}^0 – Initial concentration of C in IL phase

C_{ez} – Concentration loading of enzyme

D_{IL}^A – Diffusion coefficient of A in IL

D_{IL}^B – Diffusion coefficient of B in IL

D_{IL}^C – Diffusion coefficient of C in IL

D_O^A – Diffusion coefficient of A in oil

D_O^B – Diffusion coefficient of B in oil

D_O^C – Diffusion coefficient of C in oil

Derivation

In this theoretical study, the thickness of silica crust was negligible. A general and slightly simpler reaction, A+B⇌C, is considered as a model here. According to our previous results [Zhang, M. et al. *J. Am. Chem. Soc.* 2017, 139, 17387–17396], we had already calculated concentration of C inside an IL pool to be

$$C(r) = \lambda\zeta^2 + \frac{2n}{r}\sinh(r/\zeta) \tag{1}$$

where all symbols *n*, ζ, *r*, etc have the same definition as those in our above earlier paper.

Under steady state conditions, the amount of product C generated in the IL pool is the same as the amount of it coming out, namely:

$$-4\pi R^2 D_{IL}^C \left.\frac{\partial C}{\partial r}\right|_{R^-} = -4\pi R^2 D_O^C \left.\frac{\partial C}{\partial r}\right|_{R^+} \tag{2}$$

Therefore, the rate of generated product C per IL pool is

$$-4\pi R^2 D_{IL}^C \left.\frac{\partial C}{\partial r}\right|_{R^-} = 8\pi n D_{IL}^C \left[\sinh(R/\zeta) - \frac{R}{\zeta}\cosh(R/\zeta)\right] \tag{3}$$

Expressing this as per amount of enzyme contained within the IL pool, ($4\pi R^3 C_{ez}/3$), this becomes

$$\frac{6nD_{IL}^C}{R^3 C_{ez}}\left[\sinh(R/\zeta) - \frac{R}{\zeta}\cosh(R/\zeta)\right] \tag{4}$$

We already know that [Zhang, M. et al. *J. Am. Chem. Soc.* 139, 17387–17396 (2017)]

$$\zeta^{-2} = \frac{K_1 B_{IL}^0}{D_{IL}^A} + \frac{K_2}{D_{IL}^C} \tag{5}$$

Since K_1 and K_2 both increase in proportion with C_{ez}, so

$$\zeta \propto 1/\sqrt{C_{ez}} \tag{6}$$

Thus, as we increase the enzyme loading, ζ becomes smaller and smaller and eventually we reach the limit of large IL pool size, $\zeta << R$. In this limit, with an increasing degree of accuracy as C_{ez} is made larger, we can approximate equation (4) to

$$\approx \frac{-3nD_{IL}^C}{\zeta R^2 C_{ez}}\left[\exp(R/\zeta)\right] \tag{7}$$

In our previous work, *n* was calculated in terms of another set of parameters u_1, v_1, w_1, u_2, v_2, and w_2, all of which are in turn expressed as functions of concentrations of product and reactants in oil phase far from the IL pool, ζ, R, diffusion coefficients and partitioning constants of product and reactants and similar predetermined parameters of the systems. Although dependency of *n* on these parameters is relatively complex, once again if $\zeta << R$ the relation simplifies a little to become

$$n = \left[\frac{\left(D_o^A A_o^0 + D_o^c C_o^0\right)\left(1 - \frac{K_1 B_{IL}^0 \zeta^2}{D_{IL}^A}\right)}{D_o^A\left(1 - \frac{K_1 B_{IL}^0 \zeta^2}{D_{IL}^A}\right) + D_o^c \frac{\alpha_A}{\alpha_C}\frac{K_1 B_{IL}^0 \zeta^2}{D_{IL}^c}} - A_o^0\right]\frac{\zeta D_o^A}{D_{IL}^c}\exp(-R/\zeta) \tag{8}$$

The rate of product generated per amount of enzyme, i.e. theoretical enzyme activity, (or T_{ea}, for short) is then given by substituting (8) into equation (7) to yield

$$T_{ea} = \frac{3D_o^A}{R^2 C_{ez}}\left[A_o^0 - \frac{\left(D_o^A A_o^0 + D_o^c C_o^0\right)\left(1 - \frac{K_1 B_{IL}^0 \zeta^2}{D_{IL}^A}\right)}{D_o^A\left(1 - \frac{K_1 B_{IL}^0 \zeta^2}{D_{IL}^A}\right) + D_o^c \frac{\alpha_A}{\alpha_C}\frac{K_1 B_{IL}^0 \zeta^2}{D_{IL}^c}}\right] \tag{9}$$

Now we note that since $K_1 \propto C_{ez}$ and $\zeta \propto 1/\sqrt{C_{ez}}$ (equation 6), then $K_1\zeta^2$ is independent of enzyme concentration, C_{ez}.

Partition functions, diffusion coefficients and IL pool radius are also not affected by the concentration of enzyme. Therefore, it is immediately evident from (9) that the enzyme activity drops inversely with as enzyme loading, i.e. enzyme activity $\propto 1/C_{ez}$, as soon as we reach an enzyme concentration where ζ starts to become much smaller than the radius of the IL pool, R.

The parameters used in the calculations are listed as below.

R – Radius of the IL pool 28 μm

A_O^0 – Initial concentration of A in oil phase 0.1 M

B_O^0 – Initial concentration of B in oil phase 0.4 M

α_A – Partition constant of A between IL and oil 9:1

α_B – Partition constant of B between IL and oil 17:8

α_C – Partition constant of C between IL and oil 7:3

K_1 – Rate of forward reaction in IL 2.5×10^{-5} L/mol/s

K_2 – Rate of backward reaction in IL 2.1×10^{-2} L/mol/s

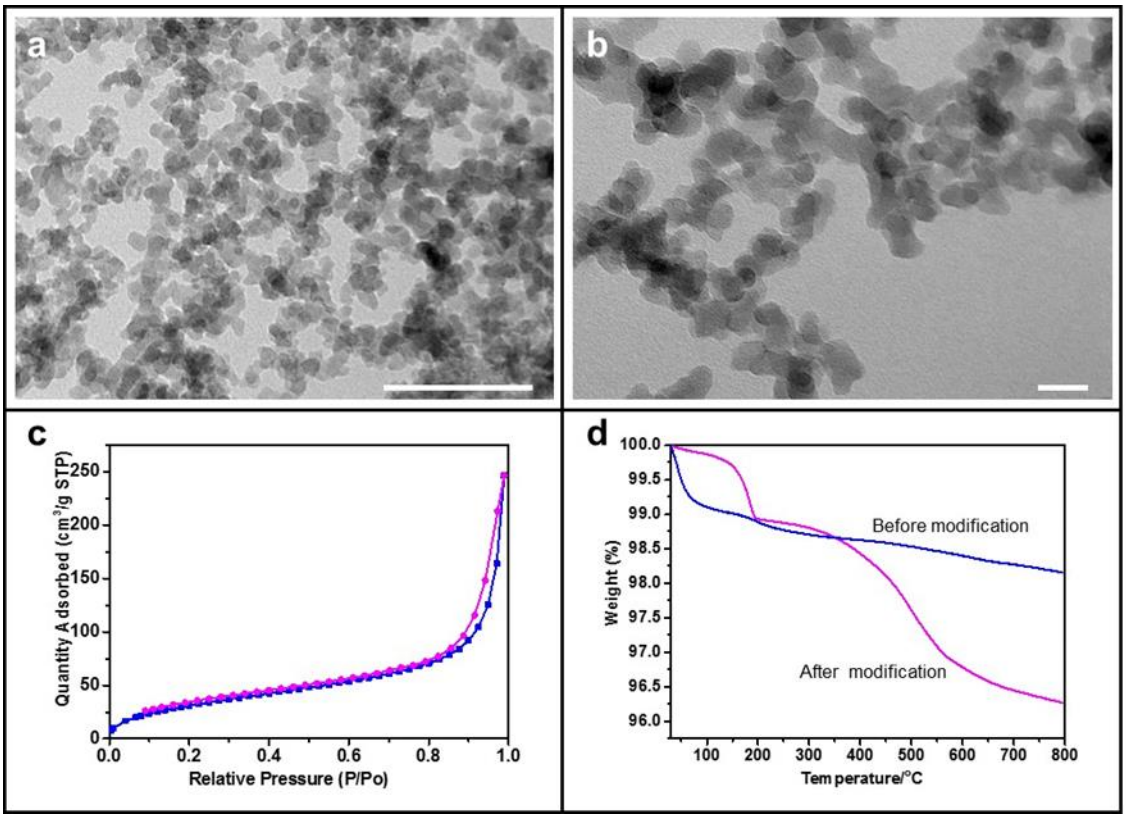

Figure S1. Characterizations of silica emulsifier. (a) TEM image, scale bar = 100 nm. (b) Magnified TEM image, scale bar = 20 nm. (c) N_2 adsorption-desorption isotherms. The specific surface area is 120 $m^2 g^{-1}$. (d) TG curves of silica particle before (blue line) and after (magenta line) hydrophobic modification.

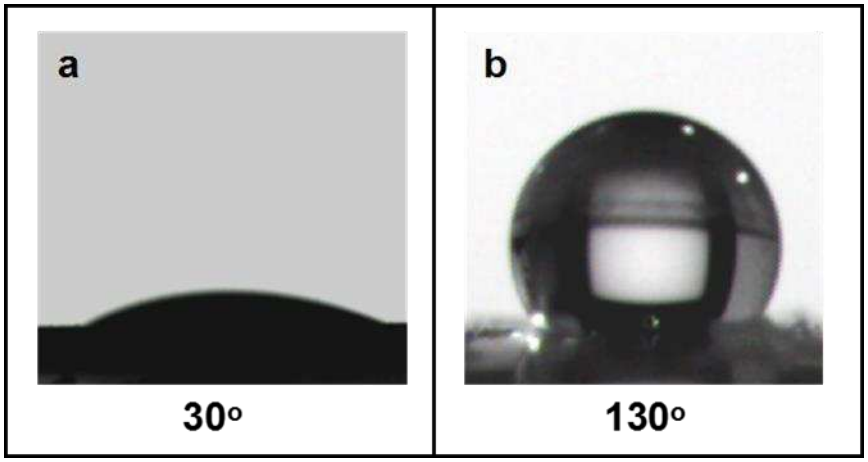

Figure S2. Appearance of a water droplet in air on a disk of compressed silica nanoparticles. Unmodified silica (a) and hydrophobically modified silica (b).

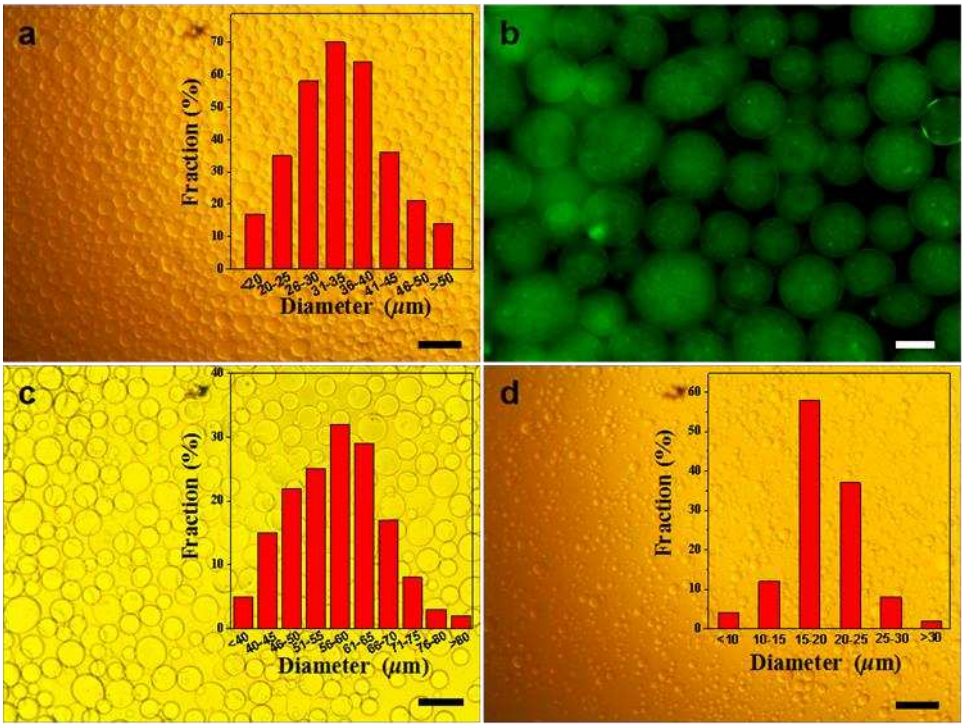

Figure S3. Optical micrographs for Pickering emulsions and their droplet size distributions. (a), (c) and (d) Scale bar = 100 μm. (b) Fluorescence confocal microscopy image with the ionic liquid phase dyed by water-soluble FITC-I, scale bar = 20 μm. Pickering emulsions were formulated at 15000 rpm (a, b), 5000 rpm (c) and 20000 rpm (d).

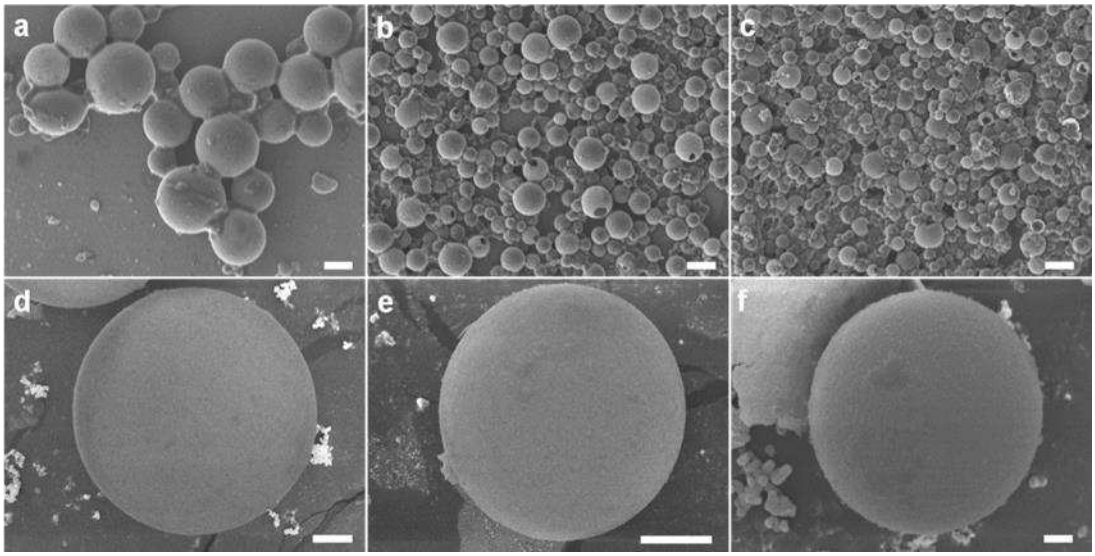

Figure S4. SEM images of liquid-solid hybrid capsules with different particle sizes fabricated by tuning the shearing speed. (a) and (d) 5000 rpm. (b) and (e) 15000 rpm. (c) and (f) 20000 rpm. Scale bar: (a, b, c) 20 μm, (d, e) 10 μm, (f) 2 μm.

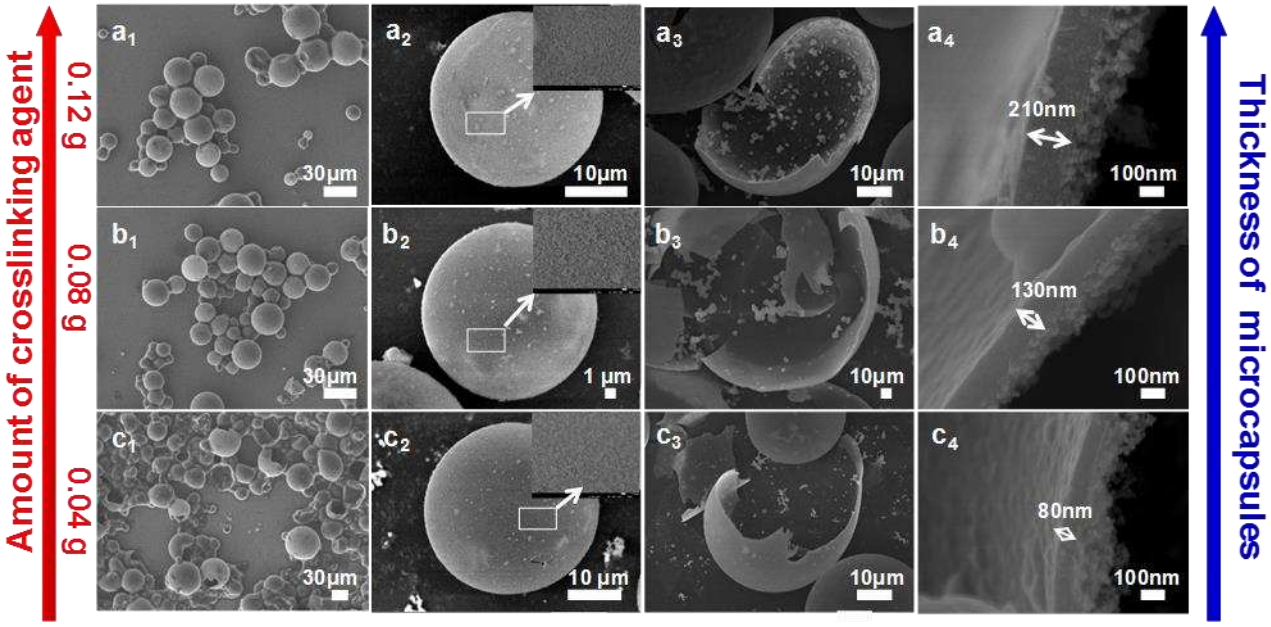

Figure S5. SEM images of the hybrid capsules with different crust thicknesses by tuning the TMS amount. (a) 0.12 g, (b) 0.08 g, (c) 0.04 g, which have average thickness of 210, 130 and 80 nm, respectively. a_1, b_1, and c_1, The capsules observed by small magnification. a_2, b_2, and c_2, A single capsule, inset is a dense outer layer of silica emulsifiers. a_3, b_3, and c_3, A single broken capsule revealing the hollow interior. a_4, b_4, and c_4, A cross-sectional view of the outer shell.

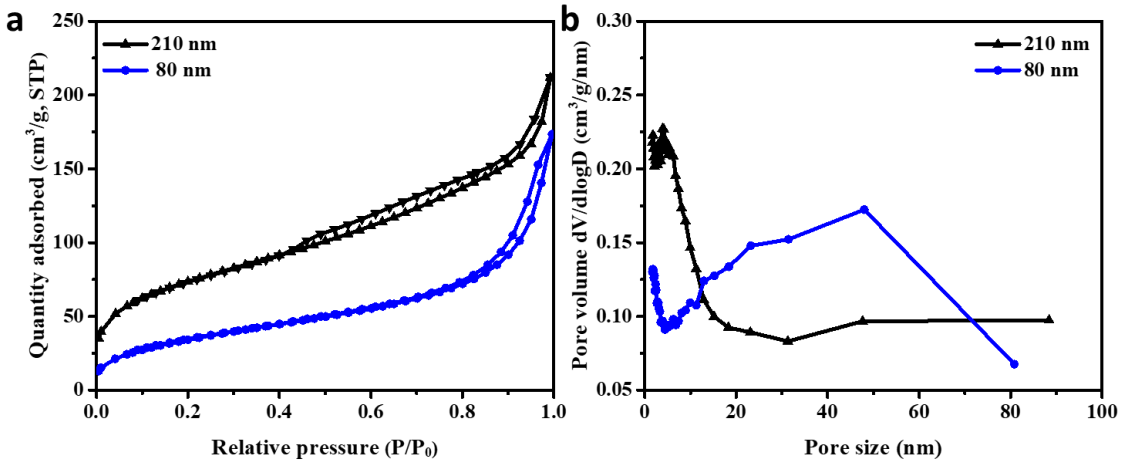

Figure S6. N_2 sorption characterization of the hybrid capsules with different crust thicknesses by tuning the TMS amount. (a) adsorption-desorption isotherms and (b) BJH pore size distribution. The specific surface areas are 128 and 268 $m^2 g^{-1}$, while the pore volumes are 0.27 and 0.33 cm^3/g, respectively, for the samples with crust thickness of 80 nm and 210 nm.

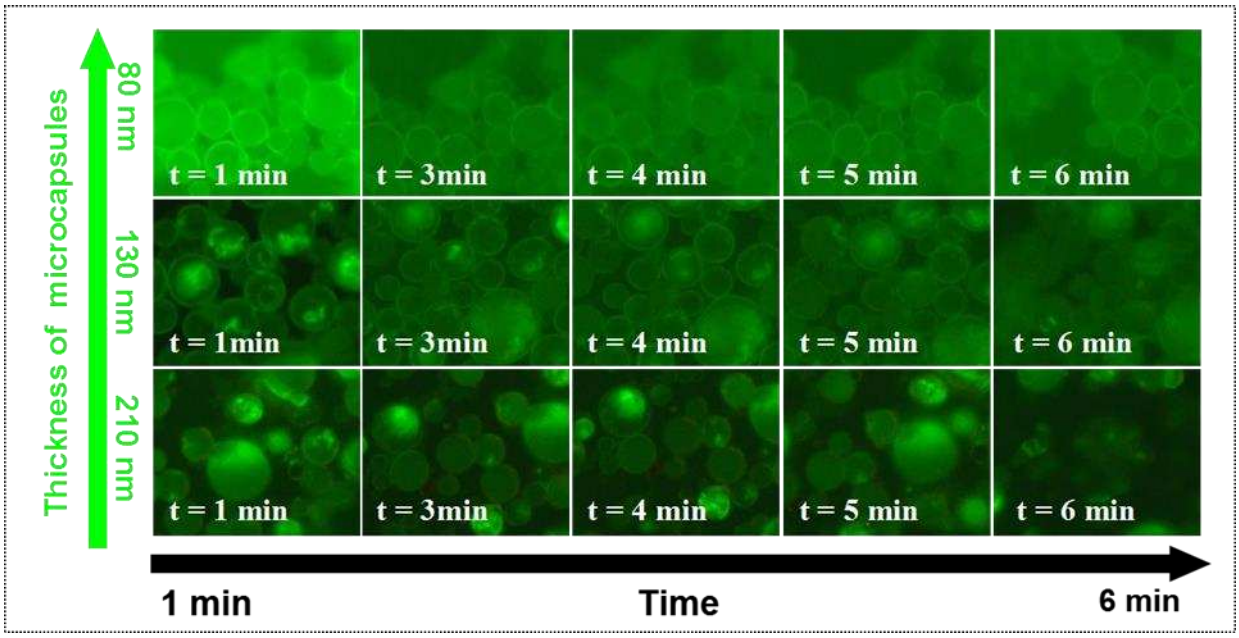

Figure S7. Fluorescence microscopy with time for the transport of FITC-I out of liquid-solid hybrid capsules. The crusts are prepared with 0.12g, 0.08 g, 0.04 g TMS, which have average thickness of 210, 130 and 80 nm, respectively.

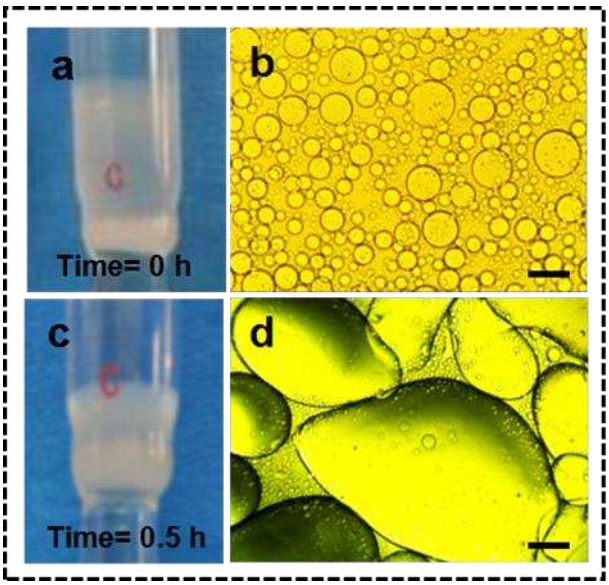

Figure S8. Flow behavior and mechanical stability for the IL-in-oil Pickering emulsion (without cross-linking) in a column. (a) and (c) Appearance of the Pickering emulsion before and after 0.5 h of flow. (b) and (d) Their optical micrographs before and after 0.5 h of flow, scale bar = 50 μm.

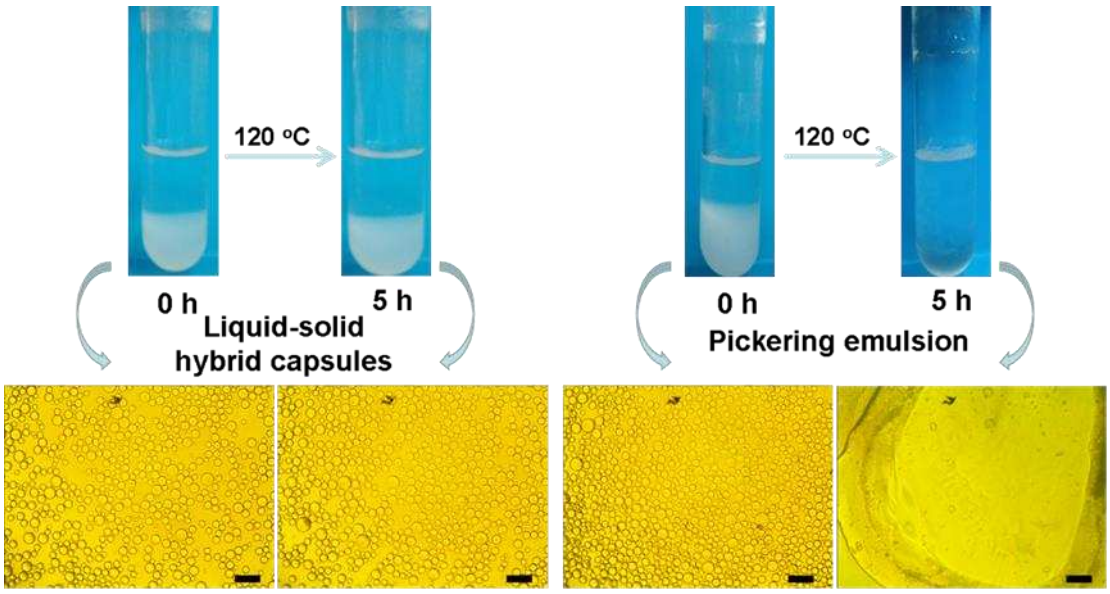

Figure S9. Comparison of thermal stability between liquid-solid hybrid capsules and the Pickering emulsion. Photographs and microscopic images of liquid-solid hybrid capsules or Pickering emulsion before (a) and after (b) thermal treatment at 120 °C. Scale bar = 100 μm.

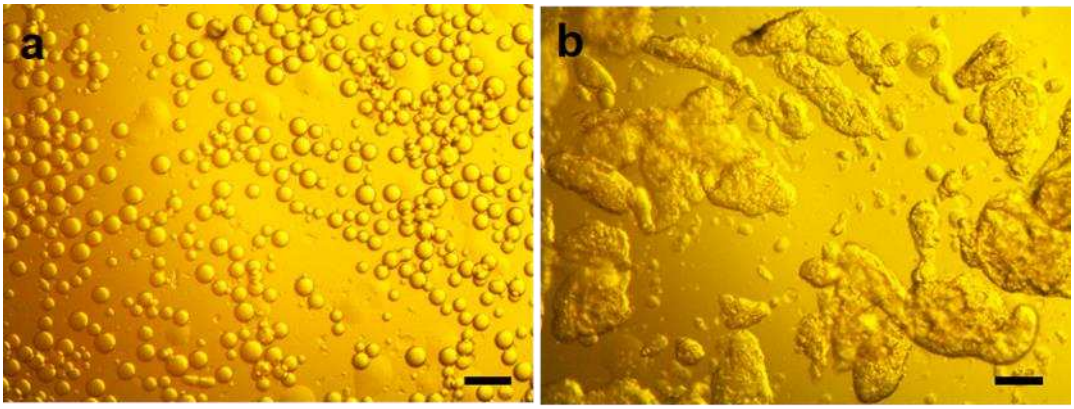

Figure S10. The behavior and tolerance of the Pickering emulsions in methanol. Microscopic images of the Pickering emulsion before (a) and after (b) stirring in methanol (30 min, 1200 rpm). Scale bar = 100 μm.

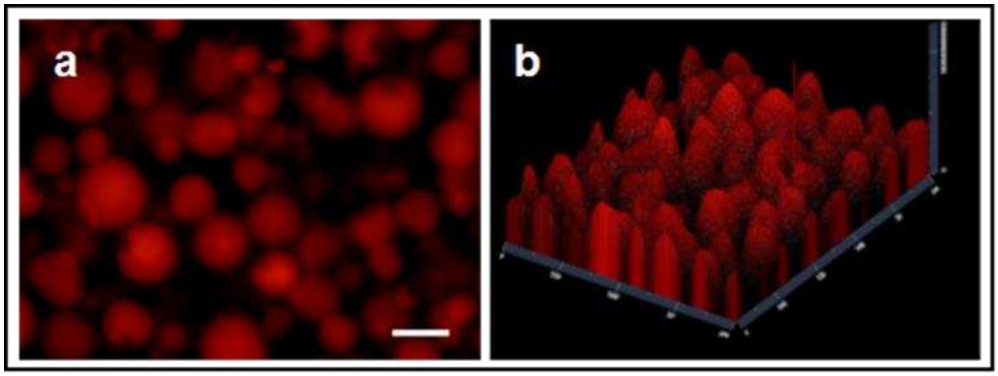

Figure S11. Confocal fluorescence microscopy for the distribution of Rhodamine B-labeled enzymes within liquid-solid hybrid capsules. 2D (a) and 3D (b) confocal fluorescence microscopies, scale bar = 50 μm.

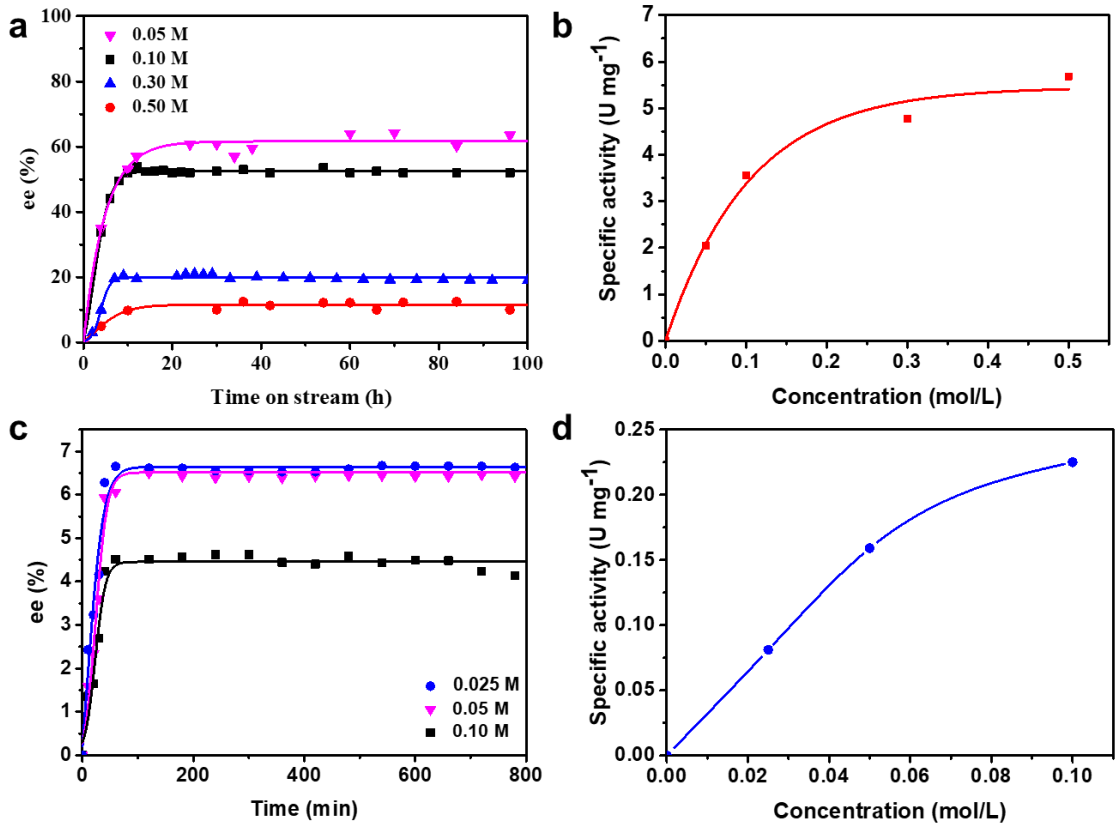

Figure S12. Kinetic profiles and specific activity for the CALB-catalyzed kinetic resolution of 1-phenylethyl alcohol over the liquid-solid hybrid catalysts in continuous-flow system and over the CALB in batch system. (a) and (b) The liquid-solid hybrid catalyst-based flow catalysis system. Reaction conditions: 1.0 g liquid-solid hybrid catalysts (CALB loading, 0.16 mg g^{-1}), The molar ratio of 1-phenylethyl alcohol to vinyl acetate is 1:4 (in *n*-octane), 45°C, 1 mL h^{-1}. (c) and (d) Batch reaction system. Reaction conditions: 1.5 g [BMIM]PF_6 and 0.4 g [Bmim]BF_4 containing 0.32 mg CALB, 1 mL *n*-octane containing 1-phenylethyl alcohol and vinyl acetate (molar ratio = 1:4), 3000 rpm, 45 °C.

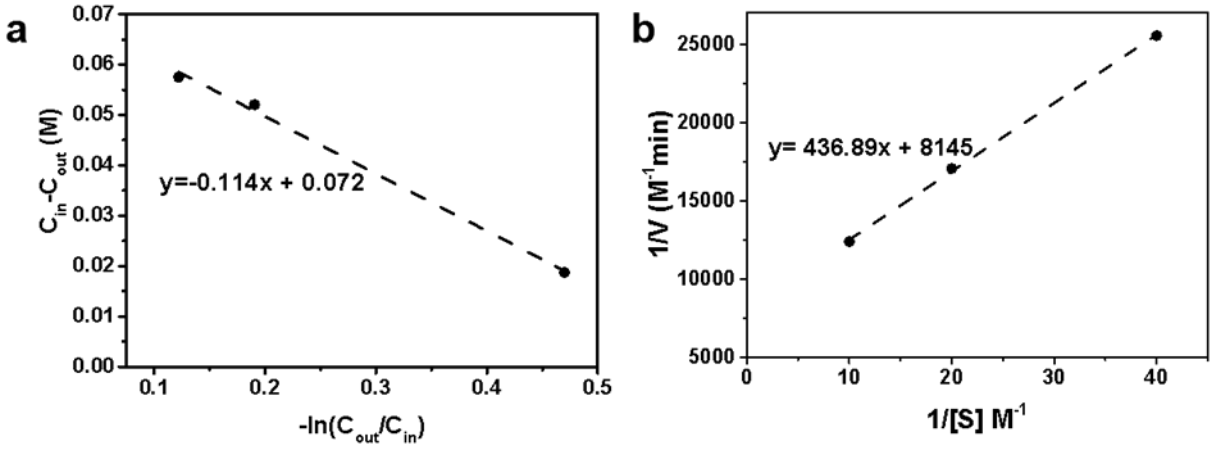

Figure S13. Lilly–Hornby plot and Lineweaver-Burk plot. (a) Lilly–Hornby plot obtained for the continuous flow reaction, flow rate = 1 mL h^{-1}. (b) Lineweaver-Burk plot obtained for the batch reaction, 3000 rpm.

Notes: Kinetic constants for the CALB in the liquid-solid hybrid catalysts based flow reaction were obtained from the Lilly-Hornby model, which was developed for the packed-bed reaction system.

$$C_{in} - C_{out} = K_m \ln \frac{C_{out}}{C_{in}} + \frac{V_{\max} V_{void}}{Q}$$

Where C_{in} and C_{out} are the reactant concentrations at the inlet and at the outlet, V_{void} is the void volume of the packed column, Q is the flow rate, K_m is the apparent Michaelis constant obtained from the slope of the plot, V_{max} is the maximal reaction rate calculated from the Y-axis intercept and the turnover number k_{cat} was calculated by V_{max}/[lipase].

The kinetic parameters Michaelis constant K_m and the maximum reaction rate V_{max} were calculated using the Lineweaver-Burk equation:

$$\frac{1}{v} = \frac{K_m}{V_{\max}[S]} + \frac{1}{V_{\max}}$$

where ν is the initial reaction rate, V_{max} is the maximal reaction rate and [S] is the concentration of the substrate.

Comparison of K_m, V_{max} and k_{cat} between liquid-solid hybrid catalysts-based continuous flow reactions and CALB in batch reactions:

	K_m (M)	V_{max} (M min^{-1})	k_{cat}(min^{-1})
Continuous flow reaction	0.11	3.2×10^{-3}	6.6×10^{3}
Batch reaction	0.05	1.23×10^{-4}	2.5×10^{2}

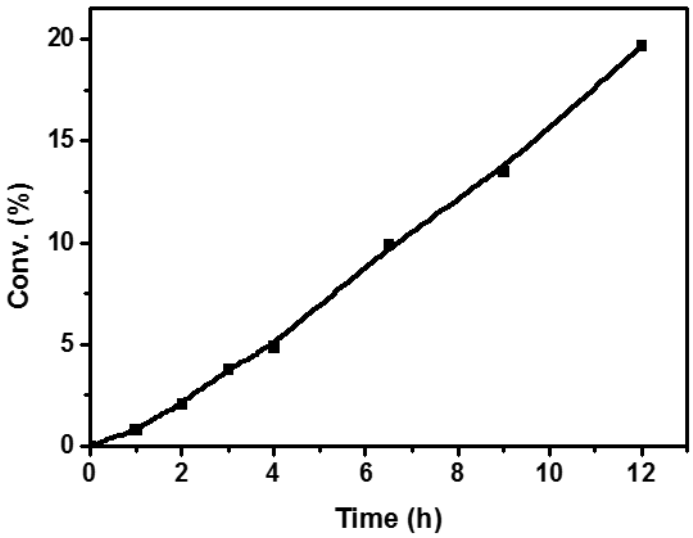

Figure S14. The kinetic plots of Cr^{III}(salen)-catalyzed ARO of cyclopentene oxide in batch reaction system. Reaction conditions: 0.8 g [BMIM]PF_6, 0.2 g [BMIM]BF_4, 30 mg Cr^{III}(salen), 2.5 mL *n*-octane solution of cyclopentene oxide (0.10 M) and $TMSN_3$ (0.11 M), 500 rpm, room temperature.

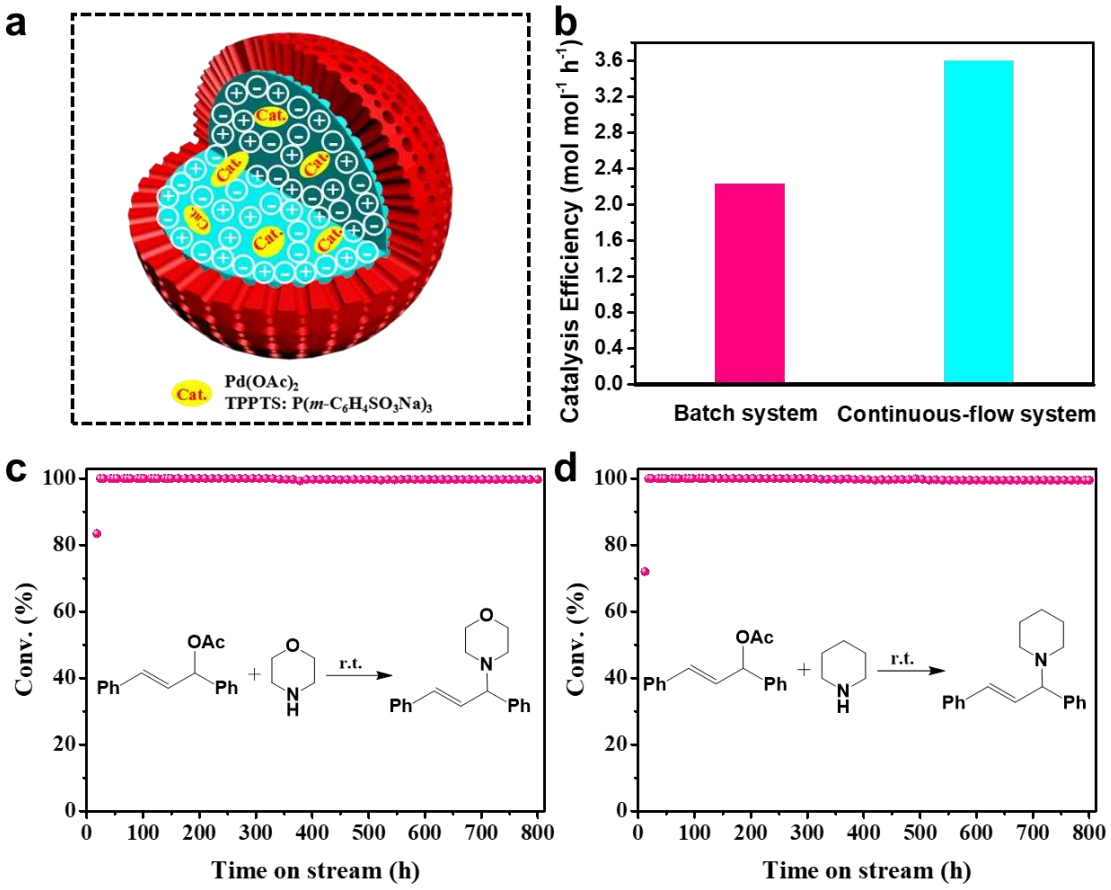

Figure S15. Pd-catalyzed allylic substitution reactions in batch system and in the liquid-solid hybrid catalyst based flow system. (a) The structure of Pd containing liquid-solid hybrid catalyst. (b) Comparison of the catalysis efficiencies in continuous-flow and batch systems using (*E*)-1,3-diphenylallyl acetate and morpholine as substrates. (c) and (d) Pd-catalyzed allylic substitution reaction over the liquid-solid hybrid catalyst with morpholine or piperidine as N-nucleophiles. Reaction conditions: liquid-solid hybrid catalysts consist of 6.0 g $[BMIM]BF_4$, 0.05 mmol $Pd(OAc)_2$, 0.20 mmol TPPTS, (*E*)-1,3-diphenylallyl acetate (0.12 M) and morpholine (0.18 M) in *n*-octane, room temperature, 1.0-1.5 mL h^{-1}.

For CALB-Catalyzed Kinetic Resolution of Alcohols

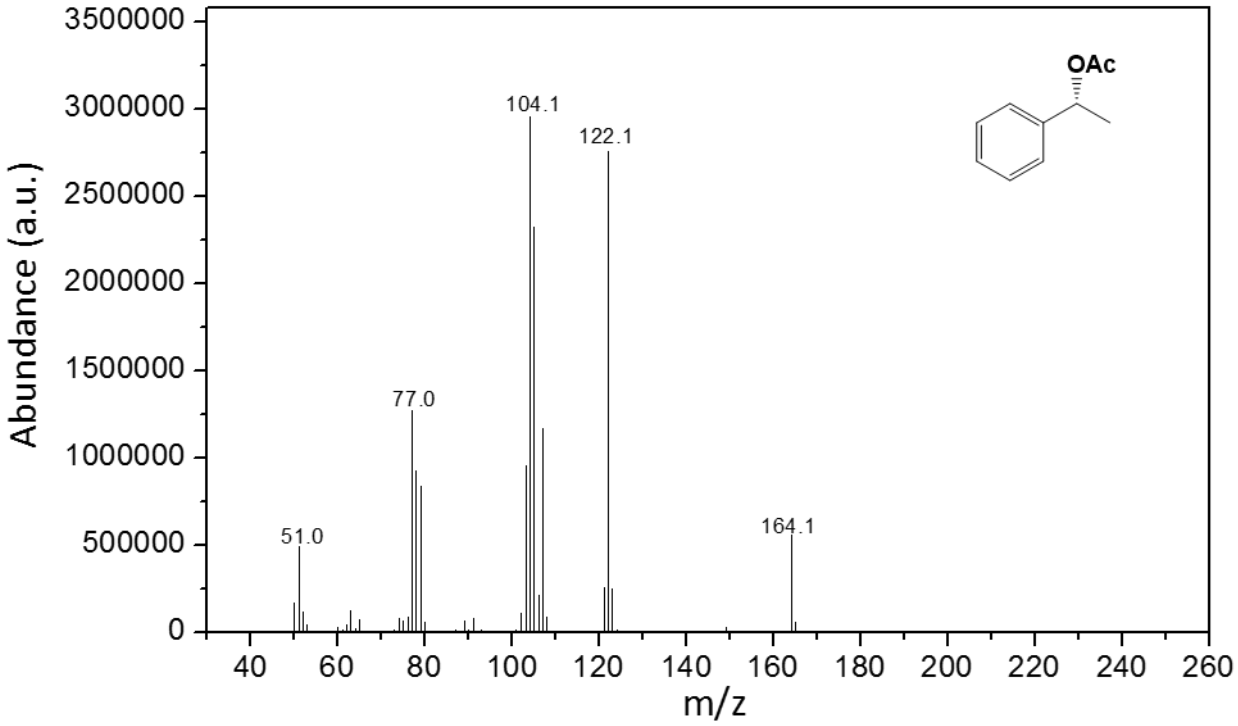

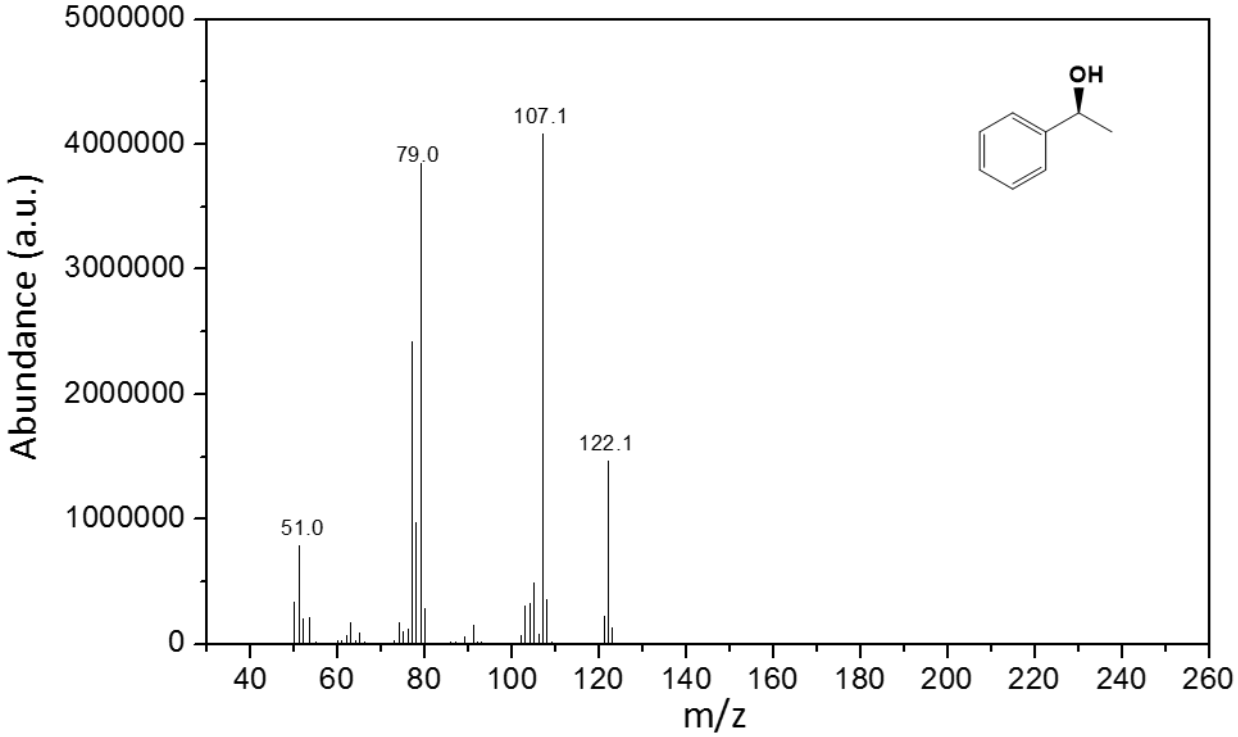

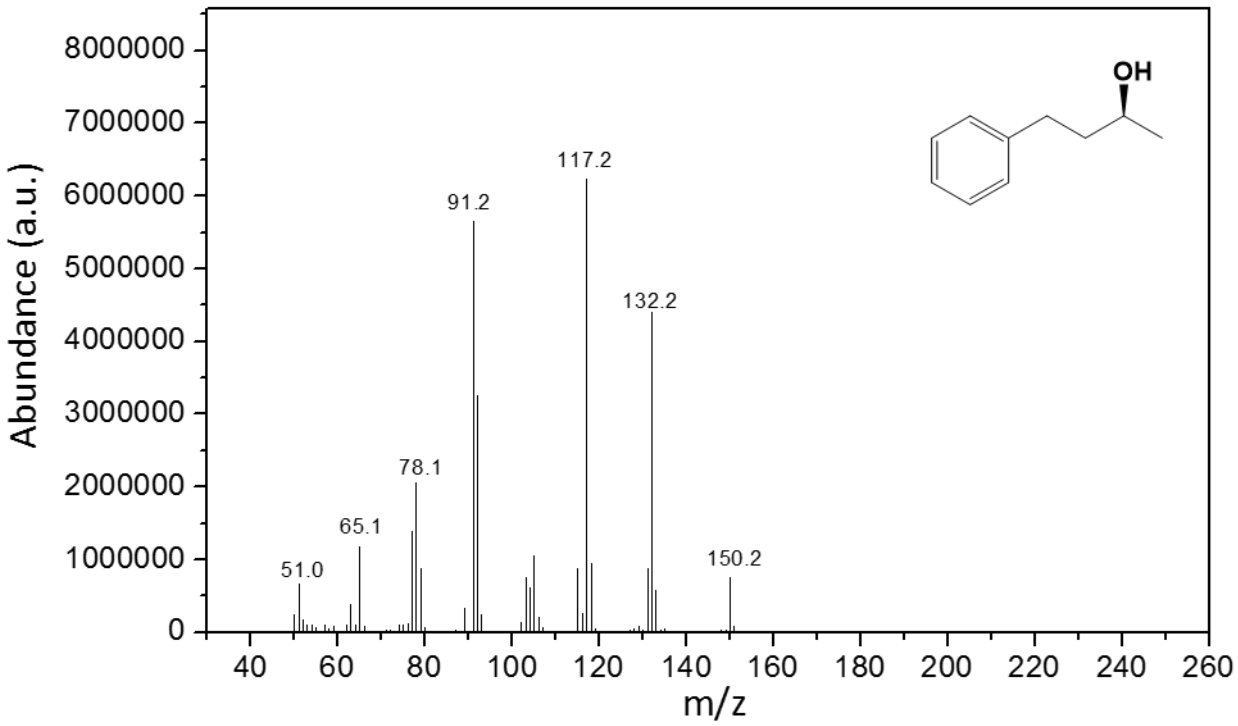
Abundance (a.u.)
m/z
OH
117.2
91.2
132.2
78.1
65.1
51.0
150.2

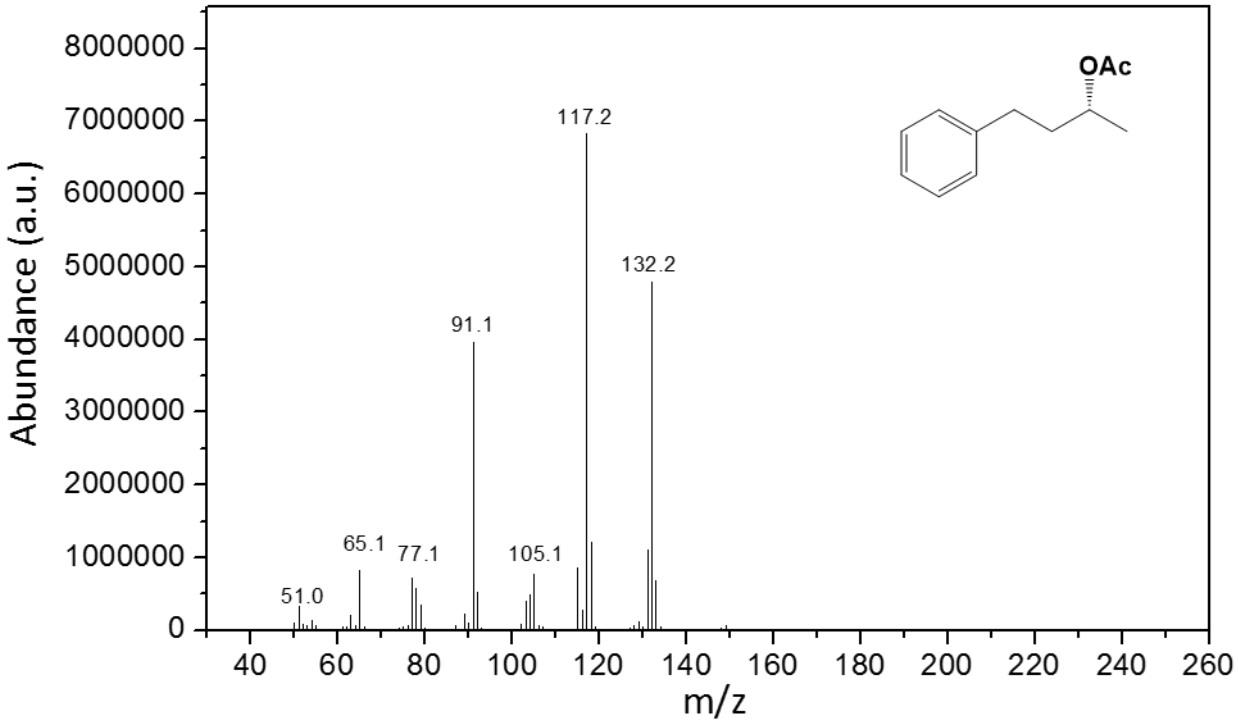
Abundance (a.u.)
m/z
OAc
117.2
132.2
91.1
65.1
77.1
105.1
51.0

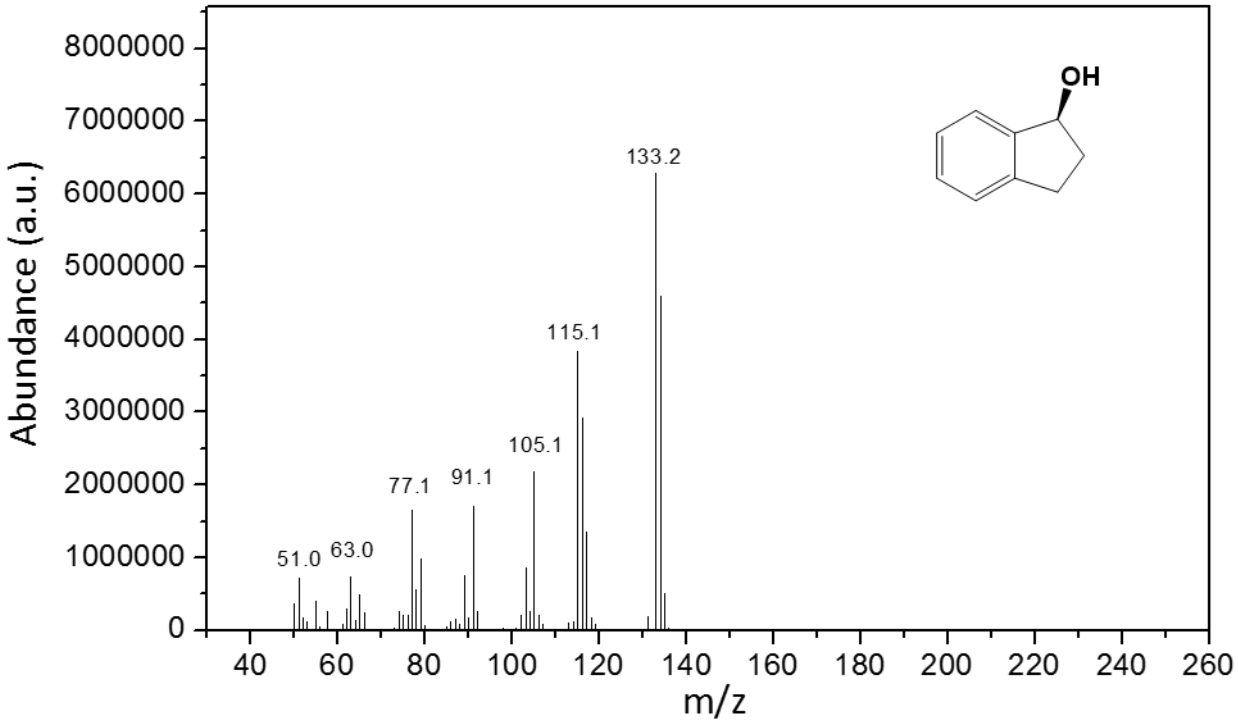
OH
133.2
115.1
105.1
91.1
77.1
63.0
51.0
Abundance (a.u.)
m/z

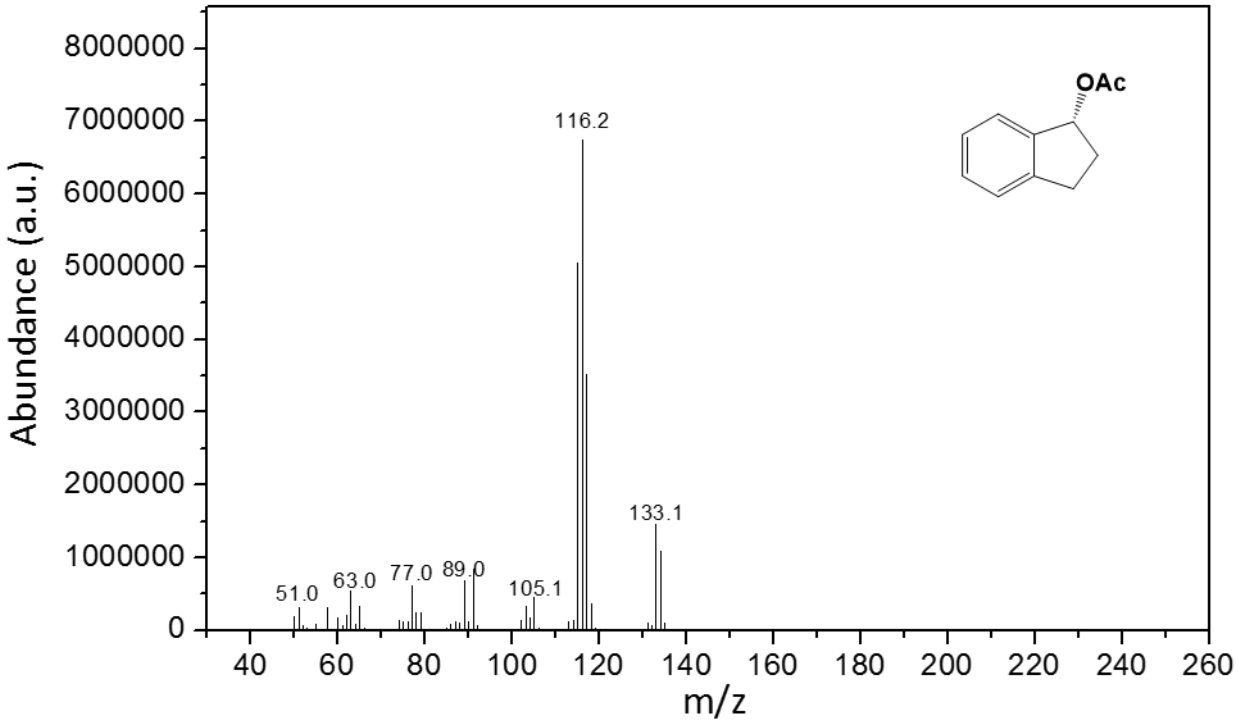
OAc
116.2
133.1
105.1
89.0
77.0
63.0
51.0
Abundance (a.u.)
m/z

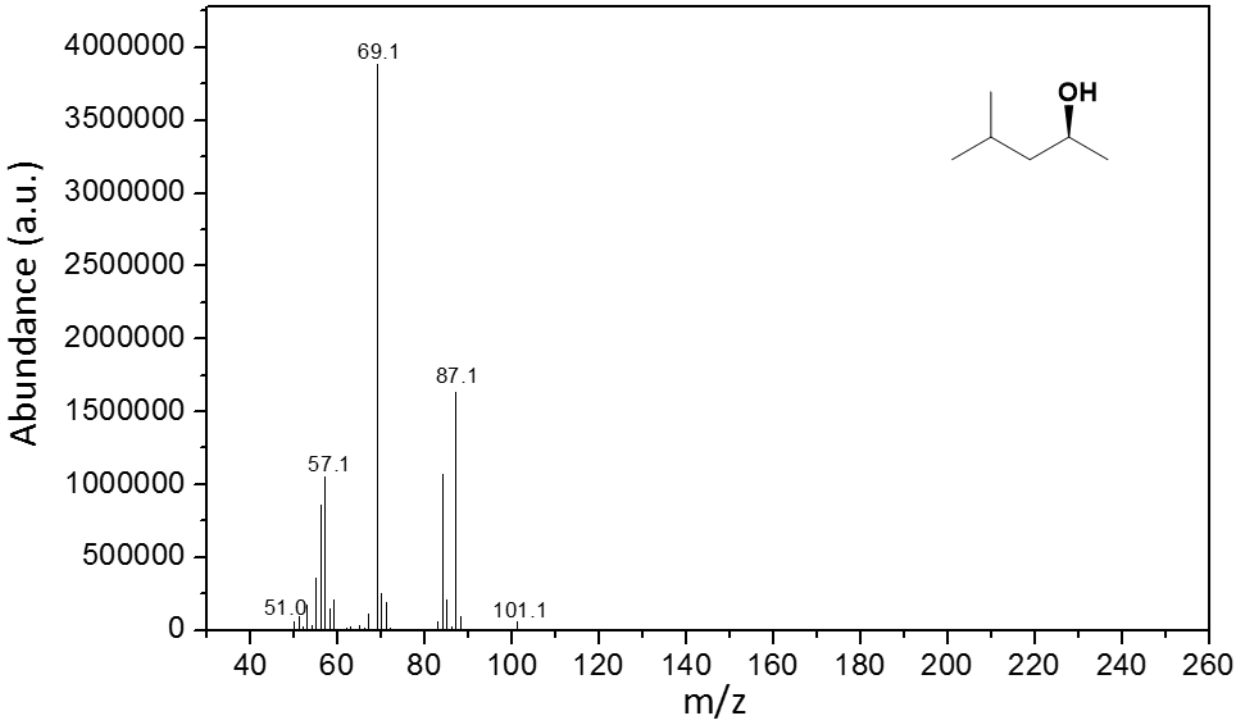
Abundance (a.u.)
m/z
69.1
87.1
57.1
51.0
101.1
OH

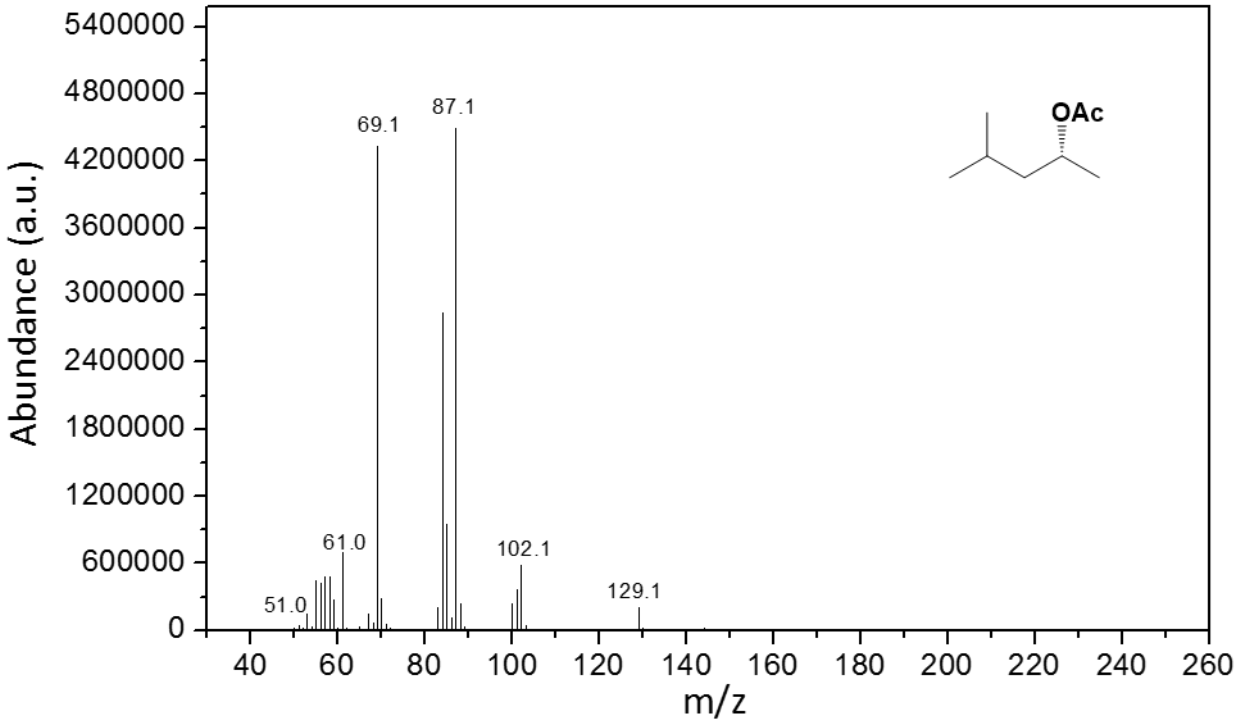
Abundance (a.u.)
m/z
69.1
87.1
61.0
51.0
102.1
129.1
OAc

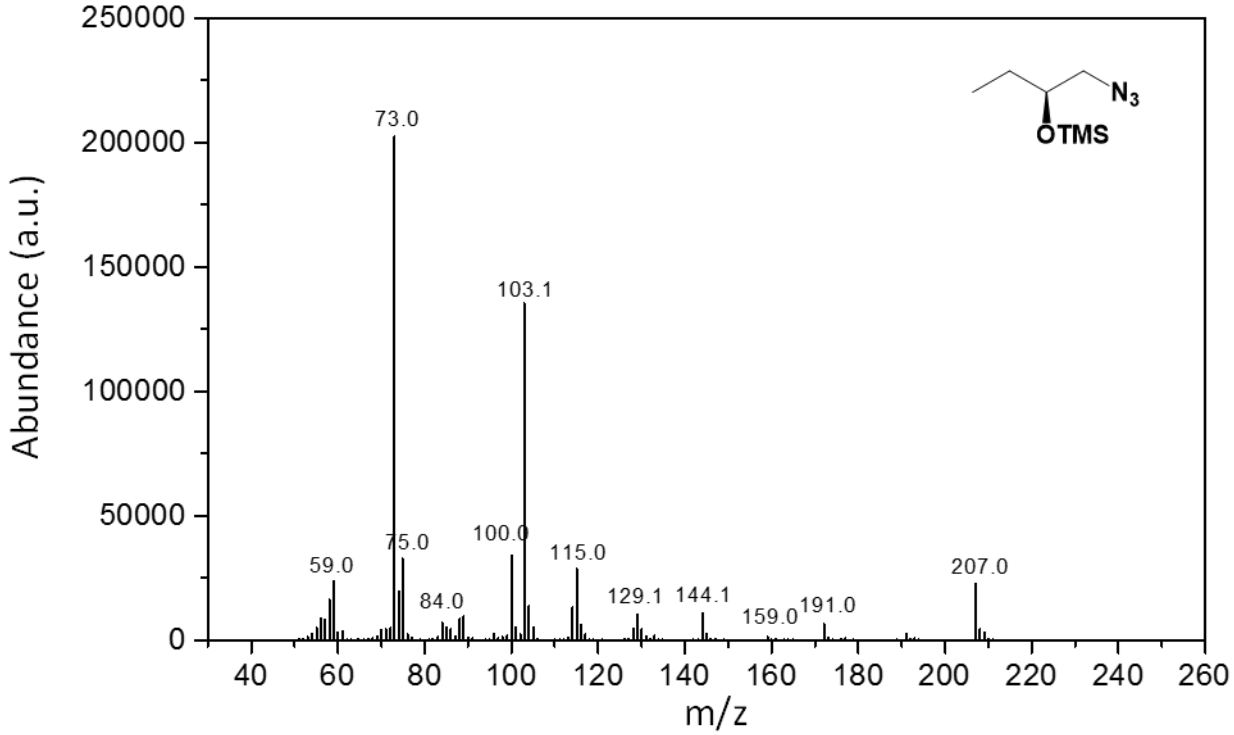
Abundance (a.u.)
m/z
73.0
103.1
59.0
75.0
84.0
100.0
115.0
129.1
144.1
159.0
191.0
207.0
N3
OTMS

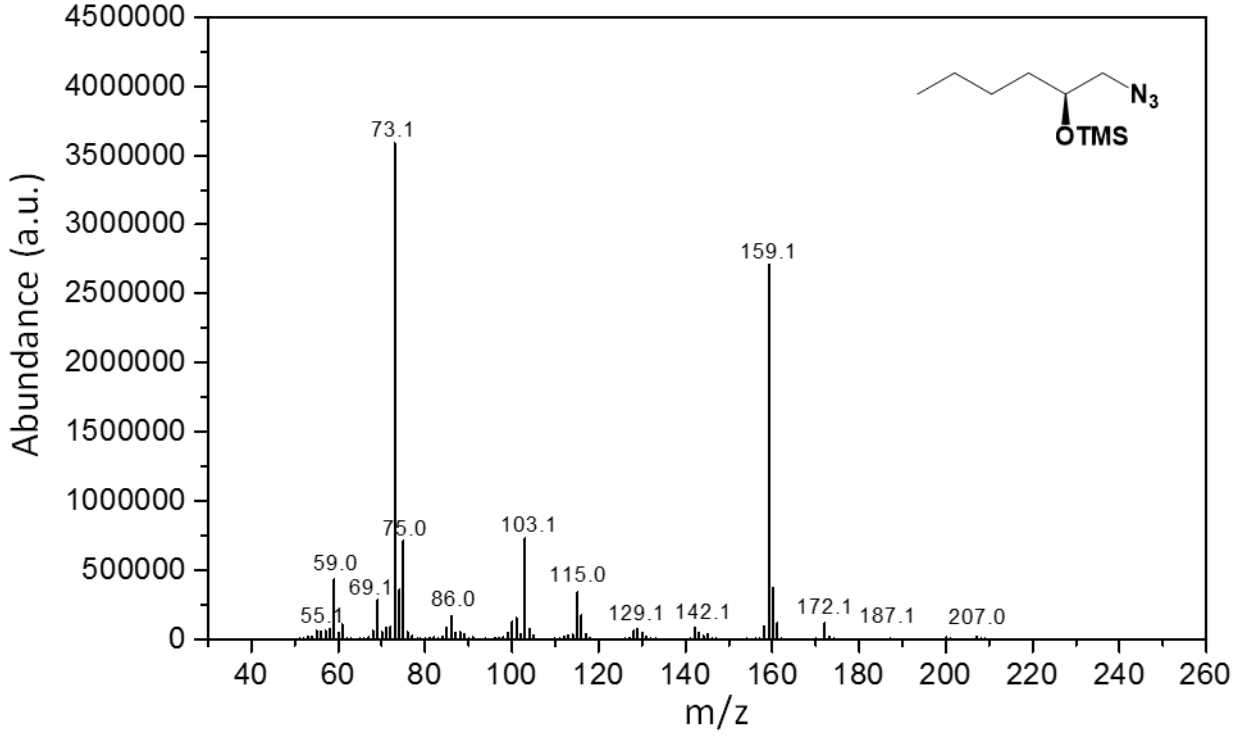
Abundance (a.u.)
m/z
73.1
159.1
75.0
103.1
59.0
69.1
55.1
86.0
115.0
129.1
142.1
172.1
187.1
207.0
N3
OTMS

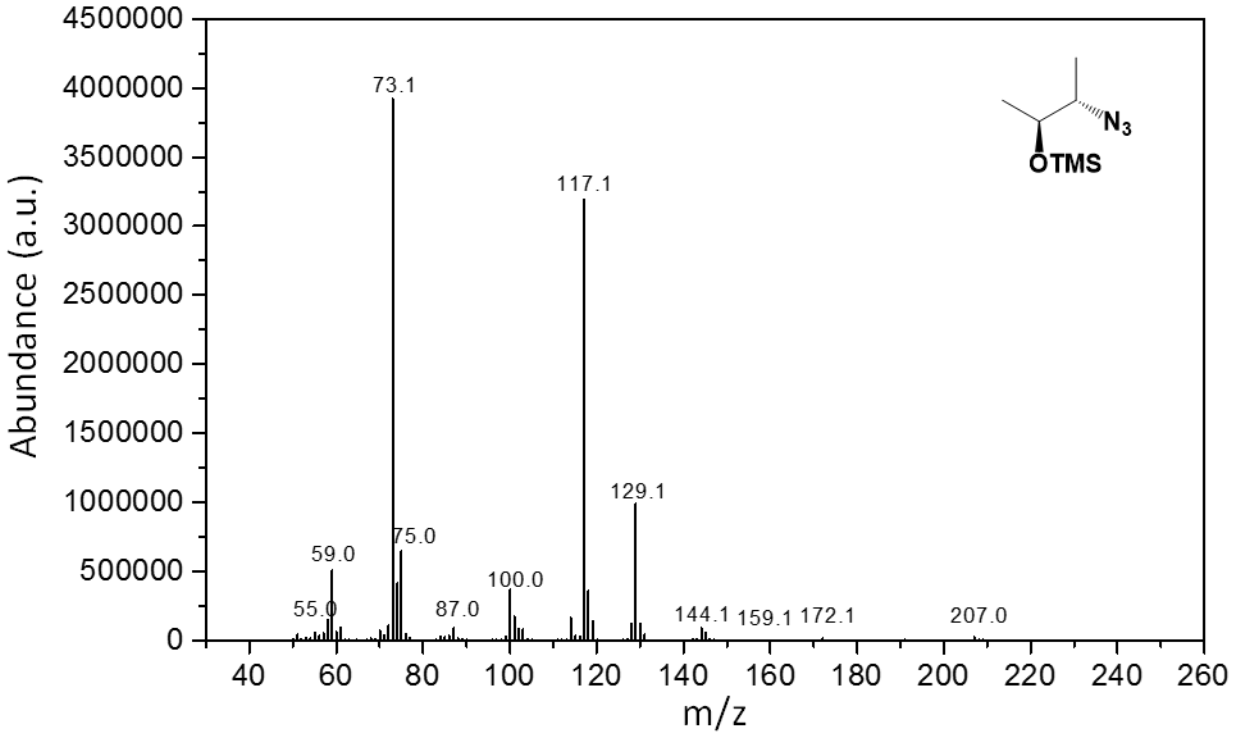
Abundance (a.u.)
m/z
73.1
117.1
129.1
75.0
59.0
100.0
55.0
87.0
144.1
159.1
172.1
207.0
N3
OTMS

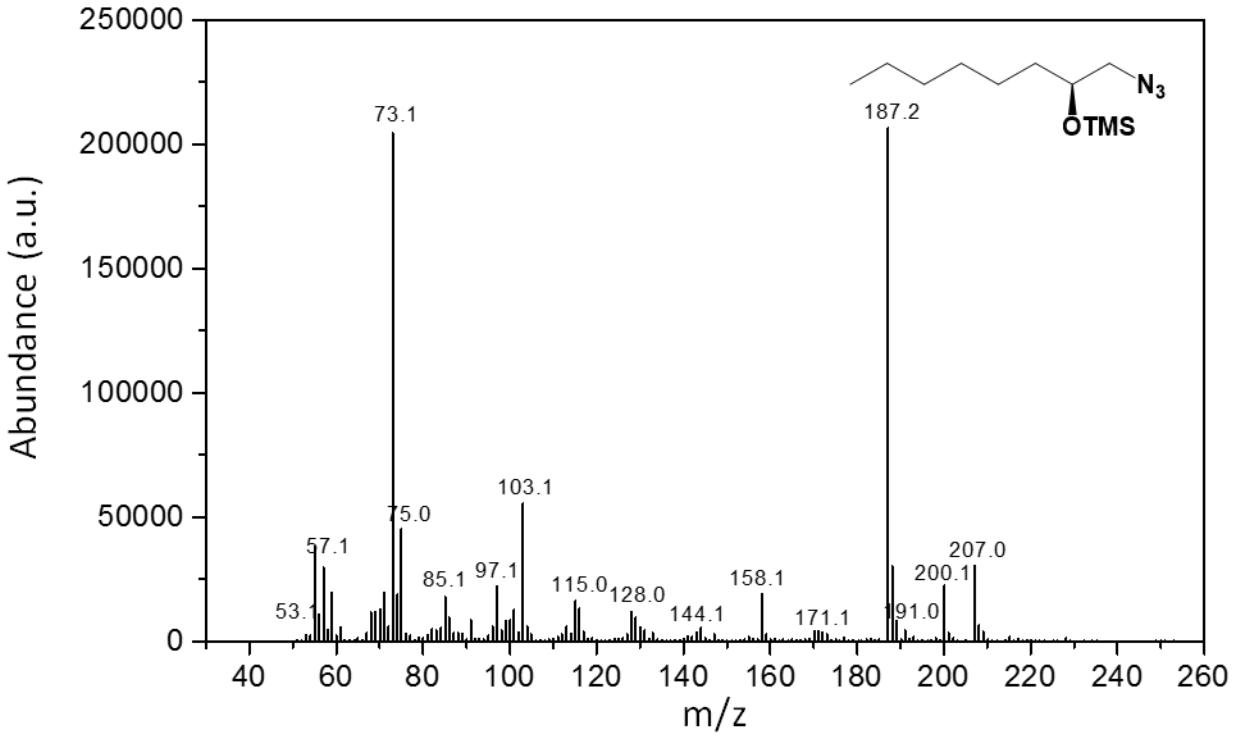
Abundance (a.u.)
m/z
73.1
187.2
103.1
75.0
57.1
85.1
97.1
115.0
128.0
158.1
144.1
171.1
191.0
207.0
200.1
53.1
N3
OTMS

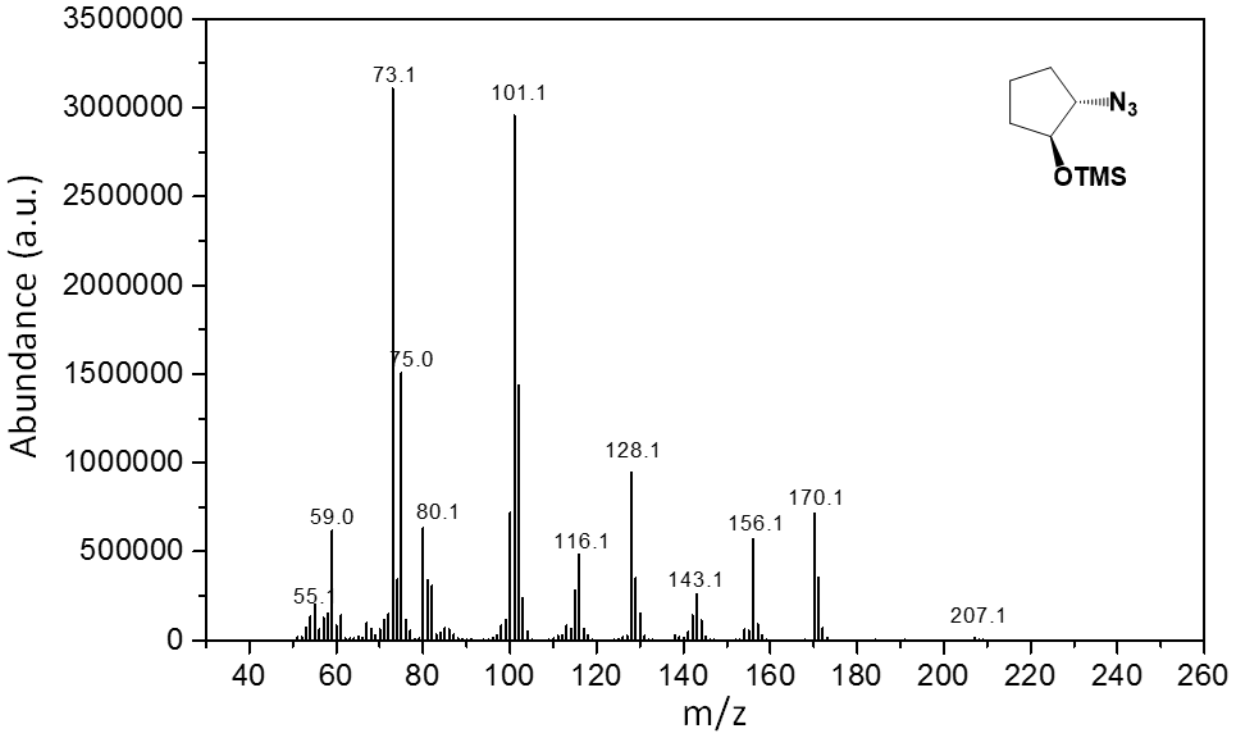
Abundance (a.u.)
m/z
73.1
101.1
75.0
128.1
59.0
80.1
116.1
156.1
170.1
143.1
55.1
207.1
N3
OTMS

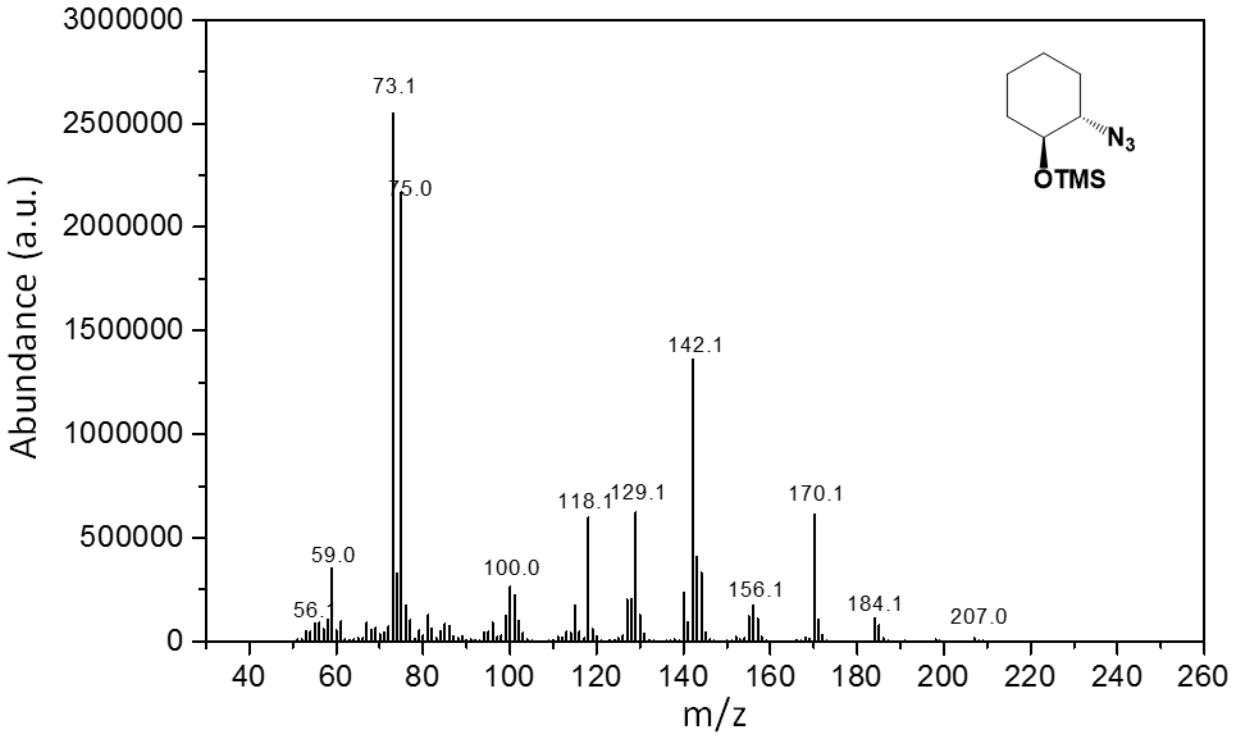
Abundance (a.u.)
m/z
73.1
75.0
142.1
118.1
129.1
170.1
59.0
100.0
156.1
184.1
56.1
207.0
N3
OTMS

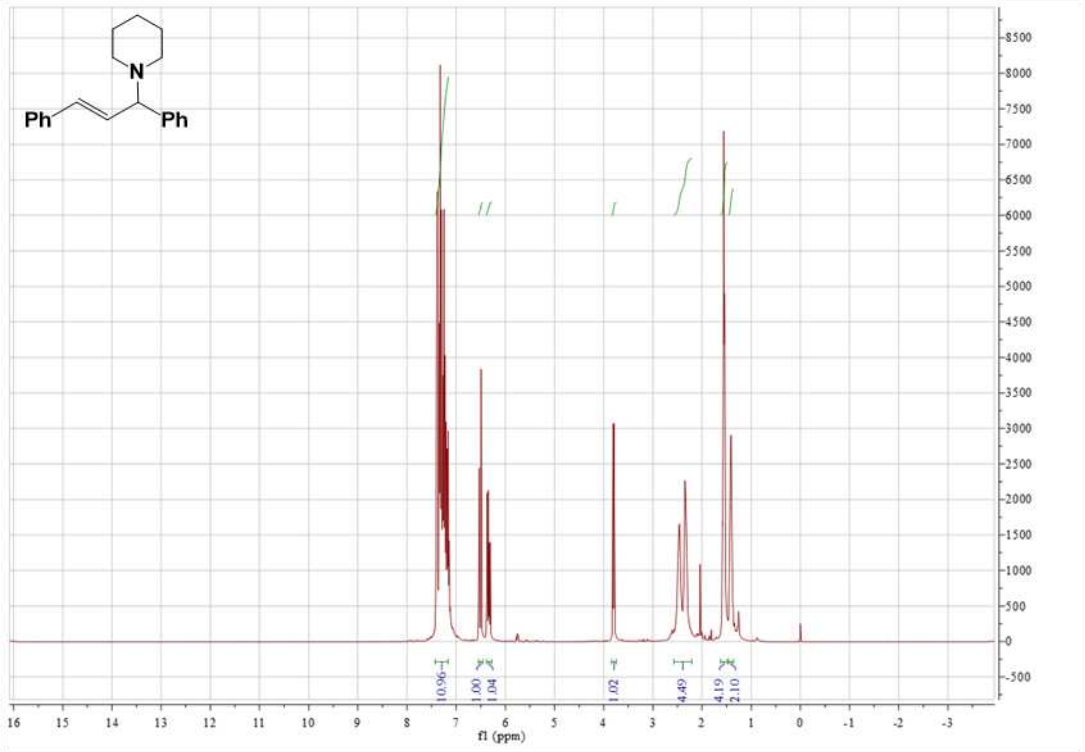
N
Ph
Ph
10.96
1.00
1.04
1.02
4.49
4.19
2.10
f1 (ppm)

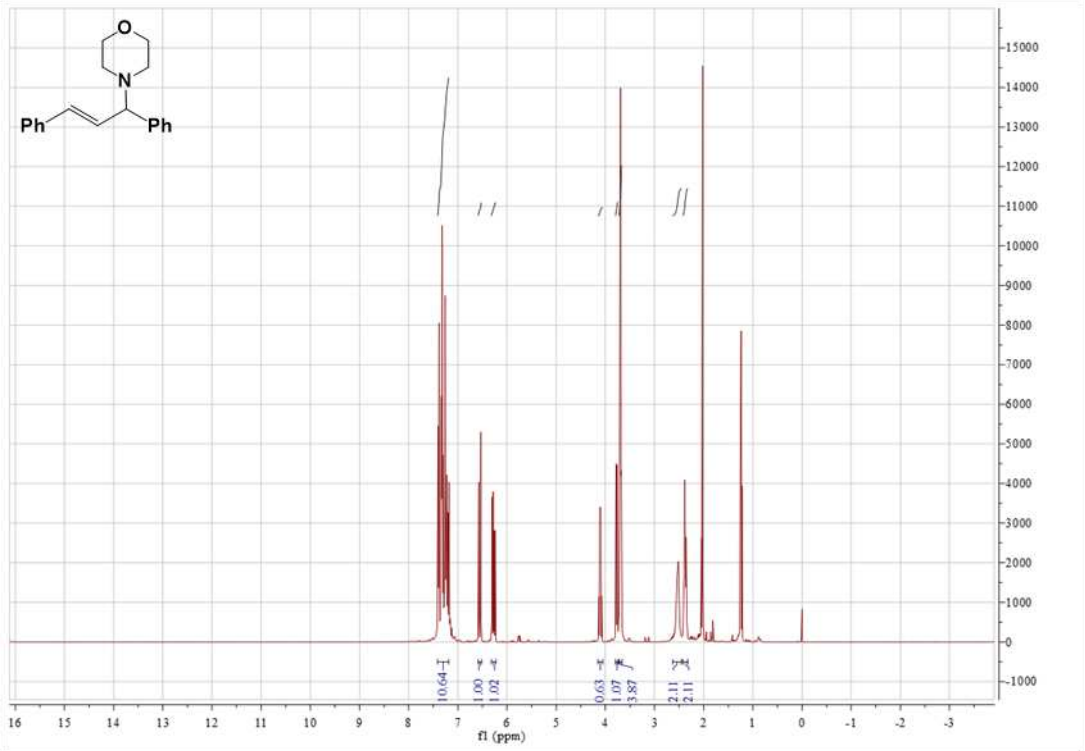
O
N
Ph
Ph
10.64
1.00
1.02
0.63
1.07
3.87
2.11
2.11
f1 (ppm)